Acta Mech 196, 87–101 (2008)
DOI 10.1007/s00707-007-0501-5
Printed in The Netherlands

Acta Mechanica

Vibration control of a simply supported cylindrical shell using a laminated piezoelectric actuator

Y. H. Zhang, S. L. Xie, X. N. Zhang

Department of Engineering Mechanics/MOE Key Laboratory for Strength and Vibration, School of Aerospace, Xi'an Jiaotong University, Xi'an, P.R. China

Received 20 January 2006; Accepted 23 July 2007; Published online 8 October 2007

Summary. This paper develops a novel laminated piezoelectric actuator (LPA) to control the vibration of a cylindrical shell structure, which is fabricated through bonding multiple piezoelectric layers of the same property together. The electromechanically coupled equations of the system are derived based on the classic shell theory. A parametric study is then conducted to evaluate the effects of geometric and physical properties of the actuator on actuating forces. The results show that as the number of layers increases, the actuating forces per voltage produced by LPA in the axial, circumferential and radial directions of the shell all increase noticeably. The active vibration control of a simply supported cylindrical shell using LPA of different layer numbers is simulated as well under a velocity feedback scheme. It is indicated that with the same control voltage the LPA can obtain a better control performance than the conventional single layer piezoelectric actuator as expected and the targeted radial modal vibration of the shell is attenuated significantly.

Nomenclature

a, b	Dimension of the actuator in the axial and circumferential direction
C_w	Transverse damping coefficient of shell
e_{31}, e_{32}	Piezo-constants of piezoelectric layer
E_b, E_p, E_s	Young's modulus of shell, piezoelectric layer and bonding layer
E_z	Electric field intensity
f_x,f_α,f_z	Actuating force in the axial, circumferential and radial direction
F_x, F_α, F_z M_{zx}, $M_{z\alpha}$	Coefficients of actuating force per voltage
M_x, M_α, $M_{x\alpha}$, $M_{\alpha x}$	Bending moments
N_x, N_α, $N_{x\alpha}$, $N_{\alpha x}$	Membrane forces
q_x, q_α, q_z	Distributed disturbance forces on the shell
Q_x, Q_α	Transverse shearing forces
R	Heaviside step function
t_p, t_s	Thickness of piezoelectric layer and bonding layer
u, v	Displacement of middle surface in the axial and circumferential direction
$V(t)$	Control voltage
w	Displacement in the radial direction
x_1, x_2, α_1, α_2	Boundary coordinates of actuator
σ_{bx}, $\sigma_{b\alpha}$, $\sigma_{bx\alpha}$	Stress components of shell

Correspondence: Y. H. Zhang, Department of Engineering Mechanics/MOE Key Laboratory for Strength and Vibration, School of Aerospace, Xi'an Jiaotong University, Xi'an 710049, P.R. China
e-mail: zyhxjtu@mail.xjtu.edu.cn

σ_{px}, $\sigma_{p\alpha}$, $\sigma_{px\alpha}$	Stress components of piezoelectric layer
σ_{sx}, $\sigma_{s\alpha}$, $\sigma_{sx\alpha}$	Stress components of bonding layer
$\varepsilon_x^{(z)}$, $\varepsilon_\alpha^{(z)}$, $\varepsilon_{x\alpha}^{(z)}$	Strain components in the curved surface parallel to the middle surface
υ_b, υ_p, υ_s	Poisson's ratio of shell, piezoelectric layer and bonding layer
ρ_b, ρ_p, ρ_s	Mass density of shell, piezoelectric layer and adhesive layer

1 Introduction

Shell structures were widely used as parts in spatial, aeronautical and automotive equipments. In these applications, undesirable vibrations of the shells may not only degrade the performance, but also influence structural integrity and reliability of the equipments. In order to ensure the safety of these equipments, the active vibration control of shell structure parts using piezoelectric actuators and sensors has been researched extensively in recent years. In reference [1], Tzou et al. gave a detailed review on the investigation of precision sensors and actuators. Tzou and his workgroup [2]–[6] have made a great deal of work on the vibration control of piezoelectric shells, their research has been extended to the vibration control of cone shells, spherical shells and to the nonlinear problems of vibration control of piezoelectric shells. Ray derived the coupled electromechanical governing equations of a simply supported shell covered entirely with piezoelectric layers on its top and bottom surfaces and analyzed the optimal control problem [7]. Balamurugan and Narayanan [8], [9] considered a plate/shell structure with thin PZT layers embedded on its top and bottom surfaces to act as distributed sensor and actuator by using the finite element method. In [10], Correia et al. researched the active control of axisymmetric shells with piezoelectric layers. In [11], Wang et al. examined the coupled electromechanical behavior of a piezoelectric actuator bonded to a finite elastic medium. The researches in [7]–[11] were focused on a one-layer piezoelectric actuator, which covered the host shell fully. However, due to the brittleness of the piezoelectric materials, it is impractical for large shell structures to have them completely covered by piezoelectric sensor and actuator layers.

In [12], Sun and Tong studied the active vibration control of the shell structures with discretely distributed piezoelectric sensors and patch actuators, each of which only covered a local area on the host shell. Wang and Vaicaitis [13] used pairs of spatially discrete piezoelectric actuators to control the vibration and noise transmission of double wall composite cylindrical shells. Whereas, even though discrete distributed actuators are properly located on the host shell, the total area covered by actuators is commonly large for gaining considerable actuating force.

According to the above reason, the area covered by an actuator should be small for feasibility. Thus, the control voltage might be high for obtaining a satisfactory control effect as well-known. However, the overhigh control voltages are not generally allowed for the safety of the system, especially for aeronautics and astronautics applications. Therefore, it seems to be limited for a traditional single layer piezoelectric actuator to increase the actuating force and improve the control performance only by increasing control voltage. Zhang [14] proposed a new piezoelectric actuator in order to obtain the desired control performance with small covered area and low control voltage. The actuator was made by laminating multiply piezoelectric layers having the same size and material constants and being applied with the same voltage to result in the consistent deformation. The active control of a beam/plate bonded with such a laminated piezoelectric actuator (LPA) has been studied in [15], [16]. The results demonstrated that the magnitudes of actuating forces per voltage produced by the actuator are larger than that of the traditional single layer actuator and thus can obtain a better control performance under the same driving voltage.

This paper extends the application of an LPA to vibration control of a cylindrical shell and is organized as followed: first, the configuration of an LPA is described and the electromechanically

coupled equations of a cylindrical shell bonding with an LPA on the top surface are derived; second, the characteristics of actuating forces exerted by an LPA are investigated based on the formulations of actuating force; third, for a simply supported cylindrical shell, the formulae of modal actuating forces of the LPA are obtained by using Galerkin's method and active vibration control of the system using LPAs of different layers, and the single layer actuator with different thickness is simulated under velocity feedback scheme; finally, a brief summary of the conclusions is given.

2 Modeling of the system

2.1 Description of the system

Figure 1 depicts the control system considered in the study, where a laminated piezoelectric actuator (LPA) is placed on the top surface of a thin elastic cylindrical shell. The configuration of the LPA is illustrated in Fig. 2. It is shown that the LPA is made up of n identical piezoelectric patches and n identical bonding layers. The piezoelectric patches are polarized along the z axis and adhered together through the surfaces of the same polarity. All piezoelectric patches in the LPA are orientated specially so as to possess the identical piezoelectric constant in the same direction. In addition, each piezoelectric patch is applied with identical control voltage. In this paper, the converse piezoelectric effect is used for active vibration control. It is assumed that all layers are bonded perfectly and the deformation of the LPA is continuous.

2.2 Governing equation of the system

The shell is of average radius of curvature r, the thickness h, and the length l. A cylindrical coordinate system is employed to describe the motion of the system. In order to facilitate the derivation of the equation of motion of the system, the following assumptions are made: (i) the total thickness of all layers is much smaller than the dimensions in the axial and circumferential directions; (ii) the shear strains in the LPA layers and base shell are negligible and (iii) the displacements are continuous and the transverse displacements w of all points on any cross-section of the system are considered to be equal. Thus, according to the geometric equations and the

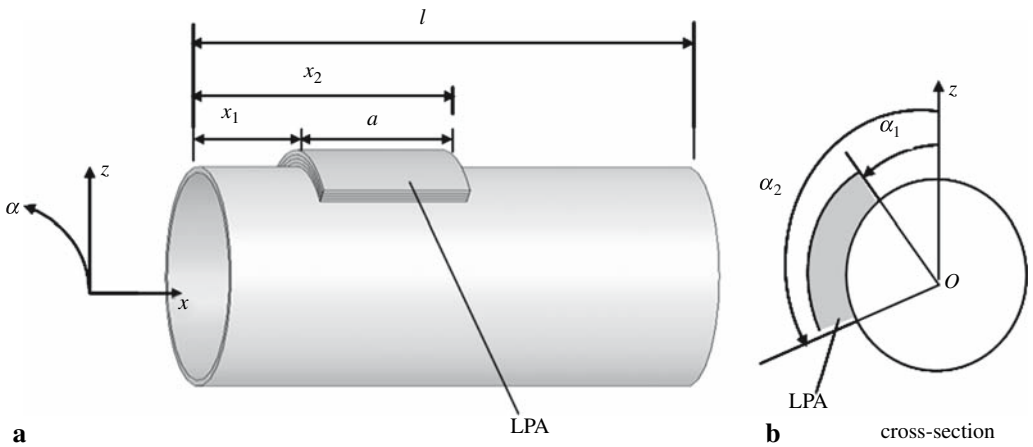

Fig. 1. The schematic of a cylindrical shell bonded with an LPA on the top surface

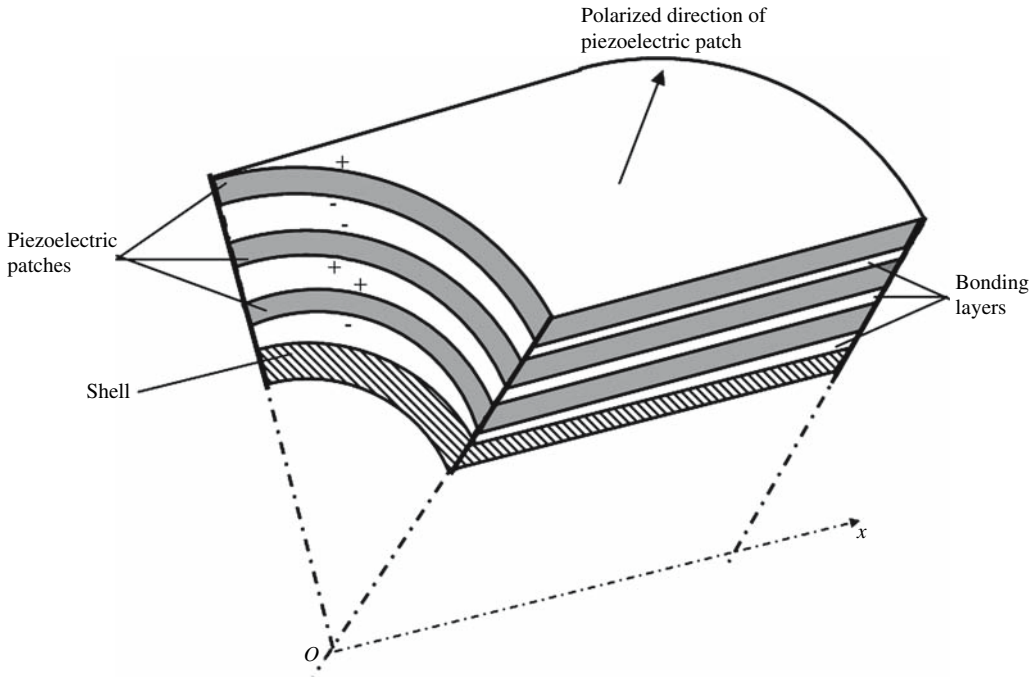

Fig. 2. Configuration of a 3-layer LPA placed on the shell

Kirchhoff hypothesis, the strain components in the curved surface that is parallel to and in a distance z away from the middle surface can be expressed as

$$\varepsilon_x^{(z)} = \varepsilon_x + k_x z, \tag{1.1}$$

$$\varepsilon_\alpha^{(z)} = \frac{1}{1+(z/r)}(\varepsilon_\alpha + k_\alpha z), \tag{1.2}$$

$$\varepsilon_{x\alpha}^{(z)} = \frac{1}{1+(z/r)}\left[\varepsilon_{x\alpha} + 2\left(1+\frac{z}{2r}\right)k_{x\alpha} z\right], \tag{1.3}$$

where ε_x, ε_α and $\varepsilon_{x\alpha}$ are the normal and shear strain components in the middle surface ($z = 0$), given by $\varepsilon_x = u_{,x}$, $\varepsilon_\alpha = \frac{1}{r}(v_{,\alpha} + w)$, $\varepsilon_{x\alpha} = \frac{1}{r}u_{,\alpha} + v_{,x}$. k_x, k_α and $k_{x\alpha}$ can be expressed as $k_x = -w_{,xx}$, $k_\alpha = \frac{1}{r^2}(v_{,\alpha} - w_{,x\alpha})$, $k_{x\alpha} = \frac{1}{r}v_{,x} - \frac{1}{r}w_{,x\alpha}$; the subscript, () denotes derivation calculus.

The relationships between stresses and strains are

$$\begin{Bmatrix} \sigma_{bx} \\ \sigma_{b\alpha} \\ \sigma_{bx\alpha} \end{Bmatrix} = \frac{E_b}{1-\upsilon_b^2}\begin{bmatrix} 1 & \upsilon_b & 0 \\ \upsilon_b & 1 & 0 \\ 0 & 0 & \dfrac{1-\upsilon_b}{2} \end{bmatrix}\begin{Bmatrix} \varepsilon_x^{(z)} \\ \varepsilon_\alpha^{(z)} \\ \varepsilon_{x\alpha}^{(z)} \end{Bmatrix} \tag{2}$$

for the shell, and

$$\begin{Bmatrix} \sigma_{sx} \\ \sigma_{s\alpha} \\ \sigma_{sx\alpha} \end{Bmatrix} = \frac{E_s}{1-\upsilon_s^2}\begin{bmatrix} 1 & \upsilon_s & 0 \\ \upsilon_s & 1 & 0 \\ 0 & 0 & \dfrac{1-\upsilon_s}{2} \end{bmatrix}\begin{Bmatrix} \varepsilon_x^{(z)} \\ \varepsilon_\alpha^{(z)} \\ \varepsilon_{x\alpha}^{(z)} \end{Bmatrix} \tag{3}$$

for the bonding layers of the LPA, and

$$\begin{Bmatrix} \sigma_{px} \\ \sigma_{p\alpha} \\ \sigma_{px\alpha} \end{Bmatrix} = \frac{E_p}{1-\upsilon_p^2} \begin{bmatrix} 1 & \upsilon_p & 0 \\ \upsilon_p & 1 & 0 \\ 0 & 0 & \dfrac{1-\upsilon_p}{2} \end{bmatrix} \begin{Bmatrix} \varepsilon_x^{(z)} \\ \varepsilon_\alpha^{(z)} \\ \varepsilon_{x\alpha}^{(z)} \end{Bmatrix} - \begin{Bmatrix} e_{31} \\ e_{32} \\ 0 \end{Bmatrix} E_z \tag{4}$$

for the piezoelectric layers of the LPA, respectively. For the linear thin piezoelectric patch, the electric field intensity E_z is assumed uniformly distributed along the thickness direction of the patch and it can be expressed as $E_z = \frac{V(t)}{t_p}$.

Expanding $(1+\frac{z}{r})^{-1}$ in Eq. (1) into series and omitting the higher order terms, then substituting Eq. (1) expressed by power series into Eqs. (2), (3), (4), the stress components can be expressed as

$$\begin{aligned} \sigma_{bx} &= D_b\left[\varepsilon_x + \upsilon_b\varepsilon_\alpha + z(\kappa_x^* + \upsilon_b\kappa_\alpha^*) - z^2\upsilon_b\tfrac{1}{r}\kappa_\alpha^*\right] \\ \sigma_{b\alpha} &= D_b\left[\upsilon_b\varepsilon_x + \varepsilon_\alpha + z(\upsilon_b\kappa_x^* + \kappa_\alpha^*) - z^2\tfrac{1}{r}\kappa_\alpha^*\right] \\ \sigma_{bx\alpha} &= D_b\tfrac{1-\upsilon_b}{2}\left[(1+\tfrac{z^2}{2r^2})\varepsilon_{x\alpha} + \left(2z - z^2\tfrac{1}{r}\right)\kappa_{x\alpha}^*\right] \end{aligned}, \tag{5.1}$$

$$\begin{aligned} \sigma_{sx} &= D_s\left[\varepsilon_x + \upsilon_s\varepsilon_\alpha + z(\kappa_x^* + \upsilon_s\kappa_\alpha^*) - z^2\upsilon_s\tfrac{1}{r}\kappa_\alpha^*\right] \\ \sigma_{s\alpha} &= D_s\left[\upsilon_s\varepsilon_x + \varepsilon_\alpha + z(\upsilon_s\kappa_x^* + \kappa_\alpha^*) - z^2\tfrac{1}{r}\kappa_\alpha^*\right] \\ \sigma_{sx\alpha} &= D_s\tfrac{1-\upsilon_s}{2}\left[(1+\tfrac{z^2}{2r^2})\varepsilon_{x\alpha} + \left(2z - z^2\tfrac{1}{r}\right)\kappa_{x\alpha}^*\right] \end{aligned}, \tag{5.2}$$

$$\begin{aligned} \sigma_{px} &= D_p\left[\varepsilon_x + \upsilon_s\varepsilon_\alpha + z(\kappa_x^* + \upsilon_p\kappa_\alpha^*) - z^2\upsilon_p\tfrac{1}{r}\kappa_\alpha^*\right] - e_{31}E_z \\ \sigma_{p\alpha} &= D_p\left[\upsilon_p\varepsilon_x + \varepsilon_\alpha + z(\upsilon_p\kappa_x^* + \kappa_\alpha^*) - z^2\tfrac{1}{r}\kappa_\alpha^*\right] - e_{32}E_z \\ \sigma_{px\alpha} &= D_p\tfrac{1-\upsilon_p}{2}\left[\left(1+\tfrac{z^2}{2r^2}\right)\varepsilon_{x\alpha} + \left(2z - z^2\tfrac{1}{r}\right)\kappa_{x\alpha}^*\right] \end{aligned}, \tag{5.3}$$

where $D_b = E_b/(1-\upsilon_b^2)$, $D_p = E_p/(1-\upsilon_p^2)$, $D_s = E_s/(1-\upsilon_s^2)$, $\kappa_x^* = \kappa_x = -w_{,xx}$, $\kappa_\alpha^* = \kappa_\alpha - \frac{\varepsilon_\alpha}{r} = -\frac{1}{r^2}(w_{,\alpha\alpha} + w)$, $\kappa_{x\alpha}^* = \kappa_{x\alpha} - \frac{1}{r}\frac{\varepsilon_{x\alpha}}{2} = -\frac{1}{2r^2}(w_{,\alpha} - rv_{,x} + 2rw_{,x\alpha})$.

The membrane forces N_x, N_α, $N_{x\alpha}$ as well as the bending moments M_x, M_α,$M_{x\alpha}$ in a differential element of the shell bonded with LPA can be expressed in terms of stress components

$$N_x = \int_{-\frac{h}{2}}^{\frac{h}{2}} \sigma_{bx}\left(1+\frac{z}{r}\right)dz + \left(\sum_{i=1}^{n}\int_{z_{2i-2}}^{z_{2i-1}} \sigma_{sx}\left(1+\frac{z}{r}\right)dz + \sum_{i=1}^{n}\int_{z_{2i-1}}^{z_{2i}} \sigma_{px}\left(1+\frac{z}{r}\right)dz\right)R, \tag{6.1}$$

$$N_\alpha = \int_{-\frac{h}{2}}^{\frac{h}{2}} \sigma_{b\alpha}dz + \left(\sum_{i=1}^{n}\int_{z_{2i-2}}^{z_{2i-1}} \sigma_{s\alpha}dz + \sum_{i=1}^{n}\int_{z_{2i-1}}^{z_{2i}} \sigma_{p\alpha}dz\right)R, \tag{6.2}$$

$$N_{x\alpha} = \int_{-\frac{h}{2}}^{\frac{h}{2}} \sigma_{bx\alpha}\left(1+\frac{z}{r}\right)dz + \left(\sum_{i=1}^{n}\int_{z_{2i-2}}^{z_{2i-1}} \sigma_{sx\alpha}\left(1+\frac{z}{r}\right)dz + \sum_{i=1}^{n}\int_{z_{2i-1}}^{z_{2i}} \sigma_{px\alpha}\left(1+\frac{z}{r}\right)dz\right)R, \tag{6.3}$$

$$N_{\alpha x} = \int_{-\frac{h}{2}}^{\frac{h}{2}} \sigma_{b\alpha x}dz + \left(\sum_{i=1}^{n}\int_{z_{2i-2}}^{z_{2i-1}} \sigma_{s\alpha x}dz + \sum_{i=1}^{n}\int_{z_{2i-1}}^{z_{2i}} \sigma_{p\alpha x}dz\right)R, \tag{6.4}$$

$$M_x = \int_{-\frac{h}{2}}^{\frac{h}{2}} \sigma_{bx}z\left(1+\frac{z}{r}\right)dz + \left(\sum_{i=1}^{n}\int_{z_{2i-2}}^{z_{2i-1}} \sigma_{sx}z\left(1+\frac{z}{r}\right)dz + \sum_{i=1}^{n}\int_{z_{2i-1}}^{z_{2i}} \sigma_{px}z\left(1+\frac{z}{r}\right)dz\right)R, \tag{6.5}$$

$$M_\alpha = \int_{-\frac{h}{2}}^{\frac{h}{2}} \sigma_{b\alpha} z dz + \left(\sum_{i=1}^{n} \int_{z_{2i-2}}^{z_{2i-1}} \sigma_{s\alpha} z dz + \sum_{i=1}^{n} \int_{z_{2i-1}}^{z_{2i}} \sigma_{p\alpha} z dz \right) R, \tag{6.6}$$

$$M_{x\alpha} = \int_{-\frac{h}{2}}^{\frac{h}{2}} \sigma_{bx\alpha} z \left(1 + \frac{z}{r}\right) dz + \left(\sum_{i=1}^{n} \int_{z_{2i-2}}^{z_{2i-1}} \sigma_{sx\alpha} z \left(1 + \frac{z}{r}\right) dz + \sum_{i=1}^{n} \int_{z_{2i-1}}^{z_{2i}} \sigma_{px\alpha} z \left(1 + \frac{z}{r}\right) dz \right) R, \tag{6.7}$$

$$M_{\alpha x} = \int_{-\frac{h}{2}}^{\frac{h}{2}} \sigma_{b\alpha x} z dz + \left(\sum_{i=1}^{n} \int_{z_{2i-2}}^{z_{2i-1}} \sigma_{s\alpha x} z dz + \sum_{i=1}^{n} \int_{z_{2i-1}}^{z_{2i}} \sigma_{p\alpha x} z dz \right) R, \tag{6.8}$$

where the Heaviside step function R is used to describe the position of the LPA on the shell $R(x, \alpha) = [H(x - x_1) - H(x - x_2)] \cdot [H(\alpha - \alpha_1) - H(\alpha - \alpha_2)]$.

Assume a viscous damping with damping coefficient C_w only in the radial direction. According to d'Alembert's principle, the equations of motion of the shell can be written as

$$rN_{x'x} + N_{\alpha x'\alpha} + rq_x = r\rho u_{,tt}, \tag{7.1}$$

$$N_{\alpha'\alpha} + rN_{x\alpha'x} + Q_\alpha + rq_\alpha = r\rho v_{,tt}, \tag{7.2}$$

$$rQ_{x'x} + Q_{\alpha'\alpha} - N_\alpha + rq_z - C_w w_{,t} = r\rho w_{,tt}, \tag{7.3}$$

$$rM_{x'x} + M_{\alpha x'\alpha} - rQ_x = 0, \tag{7.4}$$

$$M_{\alpha'\alpha} + rM_{x\alpha'x} - rQ_\alpha = 0, \tag{7.5}$$

$$-\frac{M_{\alpha x}}{r} + N_{x\alpha} - N_{\alpha x} = 0, \tag{7.6}$$

where $\rho = \rho_b\, h + (\rho_s\, nt_s + \rho_p\, nt_p)R$.

Substituting Eqs. (5) into Eqs. (6), then Eqs. (6) into Eqs. (7) yields the governing equations of the shell,

$$\begin{aligned}
&\rho u_{,tt} - \left\{ D_b h + R\left[D_s \left(A + \frac{B}{2r} \right) + D_p \left(\bar{A} + \frac{\bar{B}}{2r} \right) \right] \right\} u_{,xx} - \frac{R}{2r^2} \left[D_s A(1 - \upsilon_s) + D_p \bar{A}(1 - \upsilon_p) \right] u_{,x\alpha} \\
&- \frac{h}{2r^2} D_b (1 - \upsilon_b) u_{,\alpha\alpha} - \frac{R}{2r} \left[D_s (1 - \upsilon_s) \left(A + \frac{B}{2r} \right) + D_p (1 - \upsilon_p) \left(\bar{A} + \frac{\bar{B}}{2r} \right) \right] v_{,xx} \\
&- \left\{ \frac{h}{2r} D_b (1 + \upsilon_b) + \frac{R}{r} \left[D_s \upsilon_s \left(A + \frac{B}{2r} \right) + D_p \upsilon_p \left(\bar{A} + \frac{\bar{B}}{2r} \right) \right] \right\} v_{,x\alpha} \\
&- \left\{ -\frac{h^3}{12r} D_b - R\left[D_s \left(\frac{B}{2} + \frac{C}{3r} \right) + D_p \left(\frac{\bar{B}}{2} + \frac{\bar{C}}{3r} \right) \right] \right\} w_{,xxx} - \frac{R}{2r^2} \left[-BD_s(1 - \upsilon_s) - \bar{B} D_p (1 - \upsilon_p) \right] w_{,xx\alpha} \\
&- \frac{R}{2r^2} \left(-D_s \upsilon_s B - D_p \upsilon_p \bar{B} \right) w_{,x\alpha\alpha} - \left[D_b \upsilon_b \frac{h}{r} + R\left(\frac{D_s \upsilon_s}{r} A + \frac{D_p \upsilon_p}{r} \bar{A} \right) \right] w_{,x} = q_x - \left(\bar{A} + \frac{\bar{B}}{2r} \right) e_{31} E_z R_{,x},
\end{aligned} \tag{8.1}$$

$$\rho v_{,tt} - \frac{1}{2r}\left\{D_b(1+\upsilon_b)h + R\left[D_s(1+\upsilon_s)\left(A+\frac{B}{2r}\right) + D_p(1+\upsilon_p)\left(\bar{A}+\frac{\bar{B}}{2r}\right)\right]\right\}u_{,x\alpha}$$
$$-\frac{1}{r^2}\left[D_b h + R\left(D_s A + D_p\bar{A}\right)\right]v_{,\alpha\alpha}$$
$$-\left\{D_b(1-\upsilon_b)\left(\frac{h}{2}+\frac{h^3}{8r^2}\right) - \frac{R}{2}\left[D_s(1-\upsilon_s)\left(A+\frac{3B}{2r}+\frac{C}{r^2}\right) + D_p(1-\upsilon_p)\left(\bar{A}+\frac{3\bar{B}}{2r}+\frac{\bar{C}}{r^2}\right)\right]\right\}v_{,xx}$$
$$-\left\{\frac{h^3}{24r^2}D_b(-3+\upsilon_b) + R\left[-\frac{BD_s}{2r}+\frac{D_sC}{2r^2}\left(-1+\frac{\upsilon_s}{3}\right) - \frac{\bar{B}D_p}{2r}+\frac{D_p\bar{C}}{2r^2}\left(-1+\frac{\upsilon_p}{3}\right)\right]\right\}w_{,xx\alpha}$$
$$-\frac{1}{r^2}\left[D_b h + R\left(D_s A + D_p\bar{A}\right)\right]w_{,\alpha} = q_\alpha - \left(\frac{\bar{A}}{r}+\frac{\bar{B}}{2r^2}\right)e_{32}E_z R_{,\alpha}, \tag{8.2}$$

$$\rho w_{,tt} - \left\{D_b\frac{h^3}{12r} + R\left[D_s\left(\frac{B}{2}+\frac{C}{3r}\right) + D_p\left(\frac{\bar{B}}{2}+\frac{\bar{C}}{3r}\right)\right]\right\}w_{,xxx}$$
$$-\left\{-\frac{1}{r}\left[D_b\upsilon_b h + R\left(D_s\upsilon_s A + D_p\upsilon_p\bar{A}\right)\right]\right\}u_{,x} + \frac{R}{2r^2}\left(D_sB + D_p\bar{B}\right)u_{,x\alpha\alpha}$$
$$-\left\{\frac{h^3D_b}{24r^2}(3-\upsilon_b) + \frac{R}{2r}\left[D_s(1-\upsilon_s)\left(B+\frac{C}{r}\right) + D_p(1-\upsilon_p)\left(\bar{B}+\frac{\bar{C}}{r}\right)\right]\right\}v_{,xx\alpha}$$
$$-\left\{-\frac{1}{r^2}\left[D_b h + R\left(D_s A + D_p\bar{A}\right)\right]\right\}v_{,\alpha} - \left[-\frac{h^3D_b}{12} - \frac{R}{3}\left(D_sC + D_p\bar{C}\right)\right]w_{,xxxx}$$
$$-\left[-\frac{h^3D_b}{6r^2} - \frac{2R}{3r^2}\left(D_sC + D_p\bar{C}\right)\right]w_{,xx\alpha\alpha} - \left[\frac{R}{r}\left(D_sV_sB + D_p\upsilon_p\bar{B}\right)\right]w_{,xx}$$
$$-\left\{-\frac{1}{r^2}\left[D_b h + R\left(D_s A + D_p\bar{A}\right)\right]\right\}w + C_w w_{,t} = q_z + \frac{R}{r}e_{32}E_z\bar{A} - \left(\frac{\bar{B}}{2}+\frac{\bar{C}}{3r}\right)$$
$$\times e_{31}E_z R_{,xx} - \frac{\bar{B}}{2r^2}e_{32}E_z R_{,\alpha\alpha}, \tag{8.3}$$

where

$$A = nt_s, \quad \bar{A} = nt_p, B = nht_s + (n^2-n)t_st_p + n^2t_s^2, \quad \bar{B} = nt_p[n(t_s+t_p)+t_s+h],$$
$$C = \frac{1}{4}nt_s[3h^2 + 6(n-1)ht_p + 6nht_s + (8n^2-6n-2)t_st_p + (4n^2-6n+2)t_p^2 + 4n^2t_s^2],$$
$$\bar{C} = nt_p\left[\frac{3}{4}h^2 + (n^2+\frac{3}{2}n+\frac{1}{2})t_s^2 + n^2t_p^2 + \frac{3(n+1)}{2}t_sh + \frac{4n^2+3n-1}{2}t_st_p + \frac{3n}{2}t_ph\right].$$

3 Characteristics of actuating forces

From Eqs. (8), the actuating forces per voltage produced by an LPA in the axial, circumferential and radial directions, respectively, are

$$f_x = -\left(\bar{A} + \bar{B}/2r\right)e_{31}E_z R_{,x}/V(t) = F_x R_{,x}, \tag{9.1}$$

$$f_\alpha = -\left(\bar{A}/r + \bar{B}/(2r^2)\right)e_{32}E_z R_{,\alpha}/V(t) = F_\alpha R_{,\alpha}, \tag{9.2}$$

$$\begin{aligned} f_z &= \left[R/r\cdot e_{32}E_z\bar{A} - \left(\bar{B}/2 + \bar{C}/3r\right)e_{31}E_z R_{,xx} - \bar{B}/(2r^2)e_{32}E_z R_{,\alpha\alpha}\right]/V(t) \\ &= F_z R + M_{zx}R_{,xx} + M_{z\alpha}R_{,\alpha\alpha}, \end{aligned} \tag{9.3}$$

where the coefficients F_x, F_α, F_z, M_{zx} and $M_{z\alpha}$ can be expanded, respectively, as

$$F_x = -\left[n + \frac{n^2(t_s + t_p) + n(t_s + h)}{2r}\right] e_{31}, \tag{10.1}$$

$$F_\alpha = -\left[\frac{n}{r} + \frac{n^2(t_s + t_p) + n(t_s + h)}{2r^2}\right] e_{32}, \tag{10.2}$$

$$F_z = \frac{n e_{32}}{r}, \tag{10.3}$$

$$M_{zx} = -\left\{ \begin{array}{l} \dfrac{n^3 t_p^2}{3r} + \left[\dfrac{(4n^3 + 3n^2 - n)}{6r} t_s + \dfrac{n^2}{2}\left(1 + \dfrac{h}{r}\right)\right] t_p \\ + \left[\dfrac{2n^3 + 3n^2 + n}{6r} t_s^2 + \dfrac{1}{2} n(n+1)\left(1 + \dfrac{h}{r}\right) t_s + \dfrac{1}{4} n\left(2h + \dfrac{h^2}{r}\right)\right] \end{array} \right\} e_{31}, \tag{10.4}$$

$$M_{z\alpha} = -\frac{n^2(t_s + t_p) + n(t_s + h)}{2r^2} e_{32}. \tag{10.5}$$

It is shown from Eqs. (9) and (10) that all three actuating forces per voltage are relevant to both the position function (R) and the structural parameters of the actuator (including the number of layers (n), the thickness of a single piezoelectric patch (t_p) and the thickness of the bonding layer (t_s)). Given the position function R, one can evaluate the effects of these structural parameters on three actuating forces per voltage through inspecting the variations of the coefficients F_x, F_α, F_z, M_{zx} and $M_{z\alpha}$. Figure 3 shows the variations of magnitudes of F_x, F_α, F_z, M_{zx} and $M_{z\alpha}$ as n (from 1 to 8), where r = 200 mm, h = 1.5 mm, $e_{31} = e_{32}$ = 17 N/Vm, t_p = 1 mm and t_s = 0.1 mm.

It is seen in Fig. 3 that the magnitudes of F_x and F_α increase significantly with increasing the number of layers n. This indicates that actuating forces per voltage in the axial direction f_x and circumferential direction f_α can be enhanced by increasing n. Note that though it is shown in Eq. (10.1) and Eq. (10.2) that F_x and F_α are second-order polynomial functions of n, an approximately linear relationship between F_x and n, F_α and n can be observed from Fig. 3 when n is relatively small. This is because, in Eq. (10.1) and Eq. (10.2), the coefficients of n are much larger than those of n^2. From Eqs. (10.3)–(10.5), it is seen that F_z is linear with n, M_{zx} is a third-order

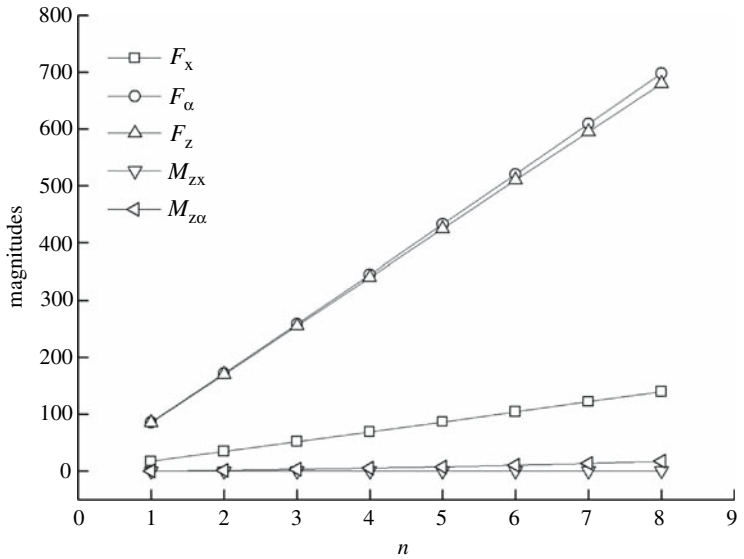

Fig. 3. Variations of F_x, F_α, F_z, M_{zx}, $M_{z\alpha}$ with the increase of layer numbers n

polynomial function of n, and $M_{z\alpha}$ is a second-order polynomial function of n. Consequently, the increase of n can pronouncedly heighten the magnitudes of F_z, M_{zx} and $M_{z\alpha}$ as shown in Fig. 3. However, it is observed, for a relatively small value of n, that the increment of F_z is much larger than the increment of M_{zx} and the increment of $M_{z\alpha}$. Thus, according to Eq. (9.3), Eq. (10.3), Eq. (10.4) and Eq. (10.5), it can be predicted that the actuating force per voltage in the radial direction f_z will increase significantly as n rises.

In addition, from Eqs. (10.1) and (10.2), it can be seen that the increase of either t_p or t_s can raise the magnitudes of F_x and F_α, and the increases of both F_x and F_α resulting from increasing t_p or t_s are much smaller than those produced by increasing n. Equation (10.3) shows that either t_p or t_s has no influence on the magnitude of F_z. Equations (10.4) and (10.5) show that the magnitudes of both M_{zx} and $M_{z\alpha}$ have an increase when either t_p or t_s increases, however, the increments of both M_{zx} and $M_{z\alpha}$ resulting from increasing t_p or t_s are very small compared with those produced by an increase of n. It implies that t_p or t_s has little influence on the actuating force per voltage in the radial direction f_z.

In summary, the actuating forces per voltage in the axial, circumferential and radial directions can be significantly enhanced only by increasing the number of layers n. Whereas both t_p and t_s have little effect on these actuating forces.

4 Active control simulations

In this Section, the vibration control of a simply supported closed cylindrical shell using LPA is simulated. The material and geometric parameters of the system studied are summarized in Table 1. The dimensions of the actuator in the axial and circumferential directions (i.e., a and b) are 40 mm and 60 mm, respectively.

The displacements of the system can be approximately expressed as

$$\begin{aligned} u &= \sum_{M=1}^{S}\sum_{N=1}^{T} U_{MN}(x,\alpha)\eta_{MN}(t), \\ v &= \sum_{M=1}^{S}\sum_{N=1}^{T} V_{MN}(x,\alpha)\beta_{MN}(t), \\ w &= \sum_{M=1}^{S}\sum_{N=1}^{T} W_{MN}(x,\alpha)\gamma_{MN}(t), \end{aligned} \tag{11}$$

where M denotes the number of the axial half-wave, N denotes the number of the circumferential wave, U_{MN}, V_{MN} and W_{MN} are the modal shape functions of the structure. For the simply supported boundary condition, we have

$$\begin{aligned} U_{MN} &= \cos\tfrac{M\pi x}{l}\cos N\alpha, \\ V_{MN} &= \sin\tfrac{M\pi x}{l}\sin N\alpha, \\ W_{MN} &= \sin\tfrac{M\pi x}{l}\cos N\alpha. \end{aligned} \tag{12}$$

Substituting Eqs. (11) and (12) into Eqs. (8) and employing Galerkin's method, where the influences of the actuator on the inertia and stiffness properties of the system are neglected and the following

Table 1. Material and geometric parameters

Shell	l = 600 mm, r_b = 200 mm, h_b = 1.5 mm, ρ_b = 7850 kg/m^3, E_b = 200 Gpa, υ_b = 0.3
Piezoelectric patches	t_p = 1 mm, E_p = 23 Gpa, υ_p = 0.3, e_{31} = e_{32} = 17 N/Vm
Bonding layer	t_s = 0.1 mm, E_s = 51 Gpa, υ_s = 0.3

non-axial-symmetric modes are taken into account: $(M, N) = (1, 1), (1, 2)$, and $(2, 1)$, yields a group of ordinary differential equations

$$\mathbf{M}\ddot{\mathbf{y}} + \mathbf{C}_d\ddot{\mathbf{y}} + \mathbf{K}\mathbf{y} = \mathbf{f}_g + \mathbf{f}_u V(t), \tag{13}$$

where $\mathbf{y} = [\boldsymbol{\eta}^T \quad \boldsymbol{\beta}^T \quad \boldsymbol{\gamma}^T]^T$ denotes the displacement vector in the modal coordinates, $\mathbf{M}$, $\mathbf{K}$ and $\mathbf{C}_d$ denote the mass matrix, stiffness matrix and damping matrix in the modal coordinates, respectively, $\mathbf{f}_g$ and $\mathbf{f}_u$ are the load vector and the actuating force vector under unit control voltage, respectively, and

$$\mathbf{f}_u = [\mathbf{f}_{u\eta}^T \quad \mathbf{f}_{u\beta}^T \quad \mathbf{f}_{u\gamma}^T]^T, \tag{14.1}$$

$$\mathbf{f}_{u\eta} = [q_{\eta 11}, q_{\eta 12}, q_{\eta 21}]^T, \quad \mathbf{f}_{u\beta} = [q_{\beta 11}, q_{\beta 12}, q_{\beta 21}]^T, \quad \mathbf{f}_{u\gamma} = [q_{\gamma 11}, q_{\gamma 12}, q_{\gamma 21}]^T, \tag{14.2}$$

where $\mathbf{f}_{u\eta}$, $\mathbf{f}_{u\beta}$ and $\mathbf{f}_{u\gamma}$ are the modal control force vectors per voltage in the axial, circumferential and axial directions, respectively, and

$$q_{\eta MN} = \int_0^{2\pi}\int_0^{l} U_{MN}(x, \alpha) f_x dx d\alpha, \tag{15.1}$$

$$q_{\beta MN} = \int_0^{2\pi}\int_0^{l} V_{MN}(x, \alpha) f_\alpha dx d\alpha, \tag{15.2}$$

$$q_{\gamma MN} = \int_0^{2\pi}\int_0^{l} W_{MN}(x, \alpha) f_z dx d\alpha. \tag{15.3}$$

Substituting Eqs. (9) and (12) into Eqs. (15) gives

$$q_{\eta MN} = F_x \int_{\alpha_1}^{\alpha_2} (U_{MN}(x_1) - U_{MN}(x_2)) d\alpha, \tag{16.1}$$

$$q_{\beta MN} = F_\alpha \int_{x_1}^{x_2} (V_{MN}(\alpha_1) - V_{MN}(\alpha_2)) dx, \tag{16.2}$$

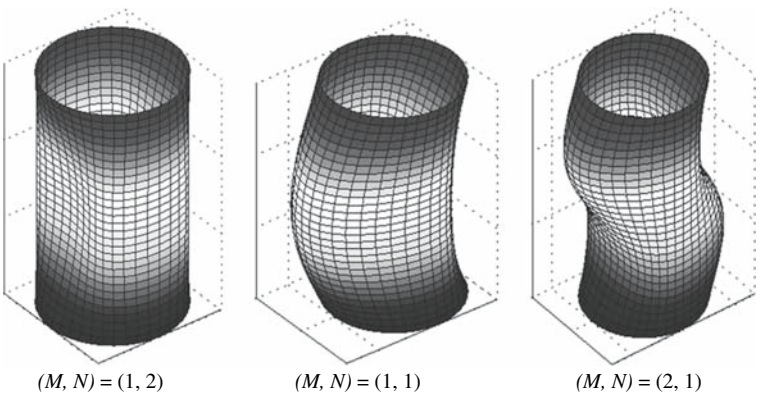

Fig. 4. Mode shapes of the system

$$q_{\gamma MN} = \left[F_z \int_{x_1}^{x_2} \int_{\alpha_1}^{\alpha_2} W_{MN} dx d\alpha + M_{zx} \int_{\alpha_1}^{\alpha_2} \left(\frac{\partial W_{MN}}{\partial x}|_{x_2} - \frac{\partial W_{MN}}{\partial x}|_{x_1} \right) d\alpha \right.$$
$$\left. = M_{z\alpha} \int_{x_1}^{x_2} \left(\frac{\partial W_{MN}}{\partial \alpha}|_{\alpha_2} - \frac{\partial W_{MN}}{\partial \alpha}|_{\alpha_1} \right) dx \right]. \tag{16.3}$$

Let the right-hand side of Eq. (13) be zero, then the modal frequencies corresponding to (M, N) = (1, 1), (1, 2) and (2, 1) can be found as 1569.3 Hz ($f_{\gamma 11}$), 764.9 Hz ($f_{\gamma 12}$) and 2997.0 Hz ($f_{\gamma 21}$), respectively, and the corresponding mode shapes are drawn in Fig. 4.

Assume the shell is subjected to a radial harmonic excitation $q_z = p_0 \delta(x - x_0)\delta(\alpha - \alpha_0) \sin(2\pi f_{\gamma 11} t)$, where $p_0 = 30\pi r\rho l$, $x_0 = \frac{l}{2}$ and α_0 = 0 are the coordinates of the excitation point. In order to obtain better control performance, according to Eq. (16.3), one can optimize the location of the actuator to maximize the modal control force $q_{\gamma 11}$ provided by the LPA for the radial mode $f_{\gamma 11}$. This can be achieved by derivating $q_{\gamma 11}$ with respect to the variables x_1, x_2, α_1 and α_2, respectively, which gives the optimal location of LPA as $x_1 = \frac{l}{2} - \frac{a}{2}, x_2 = \frac{l}{2} + \frac{a}{2}, \alpha_1 = -\frac{b}{2r}, \alpha_2 = \frac{b}{2r}$.

In this study, the velocity proportional feedback strategy was considered, thus, the control voltage is

$$V(t) = -\hat{K}\dot{w}(x_H, \alpha_H, t) = -\hat{K}\hat{\mathbf{C}}\dot{\mathbf{y}}, \tag{17}$$

where $\hat{K}$ is the control gain, (x_H, α_H) are the coordinates of the feedback measurement point, $\hat{\mathbf{C}}$ is the measurement matrix, and

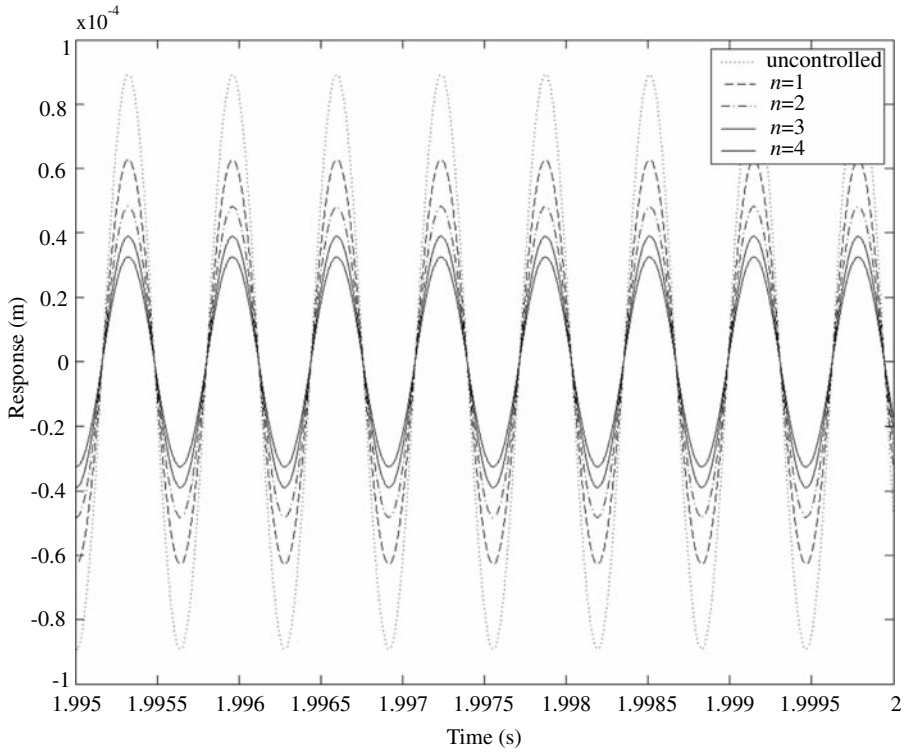

Fig. 5. Steady response of the monitored point

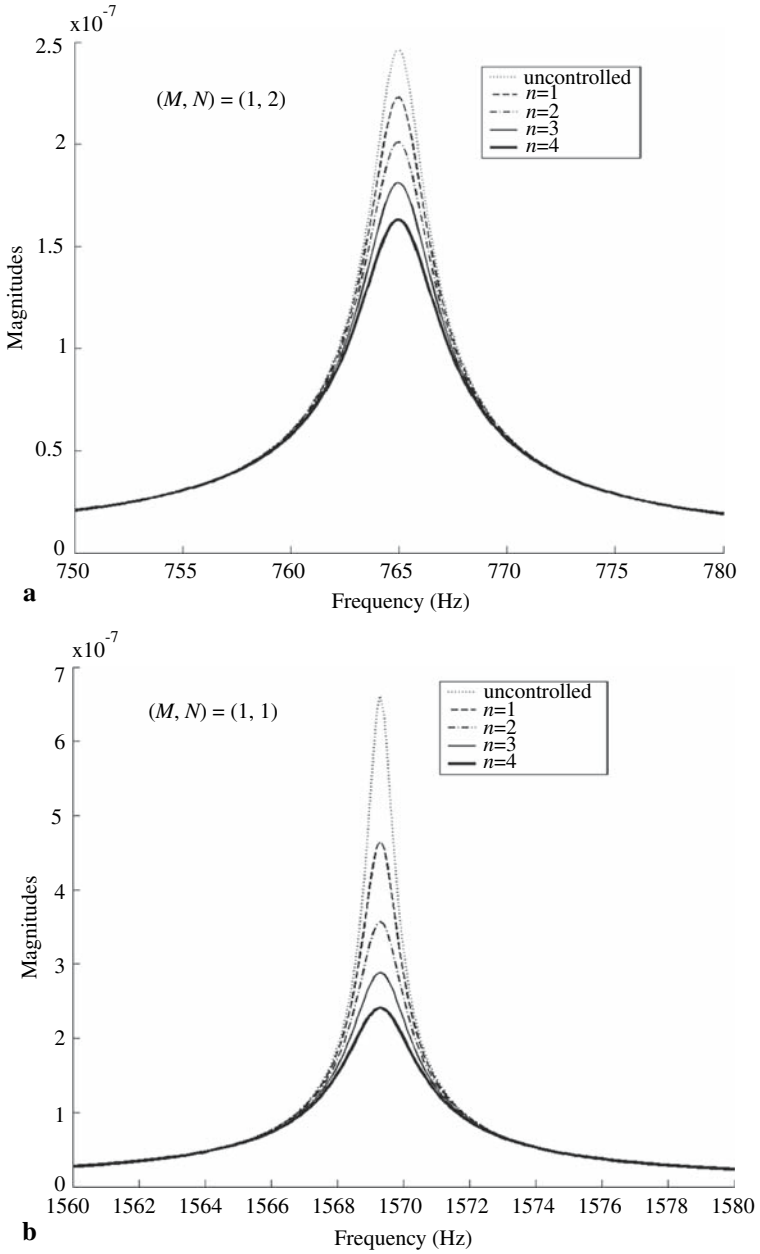

Fig. 6. Transverse displacement frequency responses

$$\hat{\mathbf{C}} = [\,0 \quad 0 \quad 0 \quad 0 \quad 0 \quad 0 \quad W_{11}(x_H, \alpha_H) \quad W_{12}(x_H, \alpha_H) \quad W_{21}(x_H, \alpha_H)\,].$$

Substituting Eq. (17) into Eq. (13) gives the closed-loop control equation of the system with velocity feedback as

$$\mathbf{M}\ddot{\mathbf{y}} + (\mathbf{C}_d + \hat{K}\mathbf{f}_u\hat{\mathbf{C}})\ddot{\mathbf{y}} + \mathbf{K}\mathbf{y} = \mathbf{f}_g. \tag{18}$$

Assume that the modal damping ratios in the radial direction are $\xi_{\gamma 11} = 2.45 \times 10^{-4}$, $\xi_{\gamma 12} = 1.60 \times 10^{-3}$, $\xi_{\gamma 21} = 4.38 \times 10^{-4}$, and the modal damping ratios in the axial and circumferential

Table 2. Damping ratios and control voltage

Number of layers	Damping ratios			Control voltage (V)
	$(M, N) = (1, 2)$	$(M, N) = (1, 1)$	$(M, N) = (2, 1)$	
$n = 0$ (uncontrolled)	1.60e-003	2.45e-004	4.38e-004	
$n = 1$	1.77e-003	3.47e-004	4.38e-004	66.82
$n = 2$	1.96e-003	4.52e-004	4.38e-004	51.35
$n = 3$	2.17e-003	5.60e-004	4.38e-004	41.50
$n = 4$	2.40e-003	6.70e-004	4.38e-004	34.69

directions are zero. The position of the feedback point is selected as $(x_H, \alpha_H) = (\frac{l}{2}, 0)$. The steady transverse displacement responses of the monitored point $(x, \alpha) = (\frac{l}{3}, \frac{\pi}{10})$ in the uncontrolled $(\hat{K} = 0)$ and controlled $(\hat{K} = 130)$ cases were calculated for different n (from 1 to 4) as shown in Fig. 5. It is observed that as the number of layers increases, the vibrational amplitude of the monitored point decreases obviously.

Figures 6a and b show the transverse displacement frequency response functions of the monitored point at frequencies near the first modal frequency ($f_{\gamma 12}$) and those near the second modal frequency ($f_{\gamma 11}$), respectively. Each figure includes the uncontrolled and controlled cases (at different layer numbers, i.e., n = 1, 2, 3 and 4). It is seen that both $f_{\gamma 12}$ and $f_{\gamma 11}$ are significantly attenuated. The amplitude of the mode $f_{\gamma 12}$ is 2.4620e-7, 2.2312e-7, 2.0166e-7, 1.8206e-7 and 1.6438e-7 for the case of n = 0 (i.e., uncontrolled), 1, 2, 3 and 4, respectively, and the amplitude of the mode $f_{\gamma 11}$ is 5.2503e-7, 4.1005e-7, 3.3051e-7, 2.7411e-7 and 2.3267e-7, respectively. Note that the amplitude of the mode $f_{\gamma 21}$ is unchanged (equals 1.5726e-7) for different cases. Referring to the mode shape of $f_{\gamma 21}$ (shown in Fig. 4), it is seen that LPA is placed just on the node-line of the mode $f_{\gamma 21}$ in the simulated system and thus has no control action on this mode. The radial mode $f_{\gamma 21}$ may be suppressed by optimizing the location of the actuator. These observations agree well with the results listed in Table 2, from which it is shown that when the number of LPA layers increases, the damping ratios of the first and second modes obviously increase but that of the third mode does not vary.

Another interesting phenomenon from Figs. 6a and b is that as n increases, the control voltage has an obvious reduction (from 66.82V at n = 1 to 34.69V at n = 4). Here, introduce a factor δ to characterize the control effect per voltage achieved by an LPA, which is defined as

$$\delta = \frac{A_0 - A_V}{A_0 \cdot V_e},$$

where A_0 is the amplitude of the response without control, A_V is the amplitude of the response under control, and V_e is the amplitude of control voltage. As the number of actuation layers increases from n = 1 (one layer) to n = 4 (four layers), the values of δ are 0.0043, 0.0087, 0.0135 and 0.0182, respectively, and the factor δ increases about 4 times ranging from 0.0043 to 0.0182. This indicates that the control performance per voltage obtained by an LPA can be improved noticeably by increasing the number of actuation layers.

Table 3. Comparison of control performance between two actuators

Actuator type	t_p (mm)	t_s (mm)	Total thickness of actuator (mm)	Amplitude of response (mm)	Control voltage (V)	δ
single-layer actuator	3.2	0.1	3.3	0.06029	66.35	0.0044
3-layer LPA	1	0.1	3.3	0.03771	41.50	0.0135

Table 4. Variation of control performance as t_p increases for a single-layer actuator

t_s (mm)	t_p (mm)	Amplitude of response (mm)	Control Voltage (V)	δ
0.1	1	0.06072	66.82	0.0043
	2	0.06052	66.60	0.0044
	3	0.06033	66.39	0.0044

Table 5. Variation of control performance as t_s increases for a single-layer actuator

t_p (mm)	t_s (mm)	Amplitude of response (mm)	Control Voltage (V)	δ
1	0.1	0.06072	66.82	0.0043
	0.2	0.06068	66.77	0.0044
	0.3	0.06064	66.73	0.0044

To further examine the actuation ability of an LPA, two different actuators are considered: one is a conventional single-layer piezoelectric actuator with a thicker layer (t_p = 3.2 mm), the other is a 3-layer LPA consisting of three thinner layers (t_p = 1 mm). The thickness of each adhesive layer is 0.1 mm, thus, two actuators possess the same total thickness (see Table 3). The steady displacement responses of the system and control voltages using two actuators were computed and compared. The results are shown in Table 3. It is seen that the 3-layer LPA obtains better vibration suppression with much smaller control voltage than the single-layer actuator. The control effect factor δ of the 3-layer LPA is about three times larger than that of the single-layer actuator. It indicates that, though with the same total thickness, the 3-layer LPA consisting of three thinner layers possesses the stronger actuation ability than the traditional single-layer piezoelectric actuator with a thicker layer.

Finally, a parametric study is carried out to evaluate the influences of the thickness of the adhesive layer (t_p) and the piezoelectric layer (t_s) on the actuation ability of a single layer actuator. Table 4 summarizes the variations of the control performance when t_p is increased from 1 mm to 3 mm while letting t_s = 0.1 mm. It is shown that the variations of the response amplitude of the monitored point, the control voltage and the control effect factor with the increase of t_p all are trivial. Table 5 gives the results when t_s is increased from 0.1 mm to 0.3 mm while letting t_p = 1 mm. Similarly, it is seen that the changes of the response amplitude, the control voltage and the control effect factor with the increase of t_s all are unobvious. These demonstrate that increasing either t_p or t_s is unable to enhance effectively the actuation force of the single-layer actuator.

5 Conclusions

In this paper, a new type of piezoelectric actuator-laminated piezoelectric actuator (LPA) was applied to the vibration control of a cylindrical shell. The electromechanically coupled equations of the system were deduced based on the classic shell theory, and the actuating forces produced by the LPA were formulated. A parametric investigation on the characteristics of the actuating forces shows that the increase of the number of LPA layers can significantly increase the magnitudes of the actuating forces per voltage in axial, circumferential and radial direction. However, both the thickness of the piezoelectric layer and the thickness of the bonding layer have little effect on the actuating forces.

The vibration controls of a simply supported closed cylindrical shell using an LPA of different layer numbers and a single-layer actuator with different thickness were also studied under the

velocity feedback strategy. The simulated results show that the targeted radial modal vibration of the cylindrical shell can be significantly suppressed using an LPA. Besides that, the control performance per voltage obtained by an LPA can be improved noticeably by increasing the number of actuation layers. Whereas, for the single-layer actuator, the improvement of the control effect by increasing the thickness of either the piezoelectric layer or the adhesive layer is marginal. Therefore, with the same total thickness, a multi-layer LPA can obtain better control performance than the conventional single-layer piezoelectric actuator.

Acknowledgements

The financial supports from the National Natural Science Foundation of China (Grant No. 50275114) and the Ministry of Education of China are gratefully acknowledged.

References

[1] Tzou, H. S., Lee, H. J., Arnold, S. M.: Smart materials, precision sensors/actuators, smart structures, and structronic systems. Mech. Adv. Mat. Struct. **2**, 367–393 (2004).
[2] Tzou, H. S., Bao, Y.: Parametric study of segmented transducers laminated on cylindrical shells, part 2: actuator patches. J. Sound Vibr. **197**, 225–249 (1996).
[3] Zhou, Y. H., Tzou, H. S.: Active control of nonlinear piezoelectric circular shallow spherical shells. Int. J. Solids Struct. **37**, 1663–1677 (2000).
[4] Tzou, H. S., Wang, D. W., Chai, W. K.: Dynamics and distributed control of conical shells laminated with full and diagonal actuators. J. Sound Vibr. **256**, 65–79 (2002).
[5] Tzou, H. S., Ding, J. H.: Optimal control of precision paraboloidal shell structronic systems. J. Sound Vibr. **276**, 273–291 (2004).
[6] Tzou, H. S.: Piezoelectric shells. Dordrecht: Kluwer Academic Publishers 1993.
[7] Ray, M. C.: Optimal control of laminated shells using piezoelectric sensor and actuator layers. AIAA **41**, 1151–1157 (2003).
[8] Balamurugan, V., Narayanan, S.: Shell finite element for smart piezoelectric composite plate/shell structures and its application to the study of active vibration control. Finite Elements Anal. Desi. **37**, 713–738 (2001).
[9] Narayanan, S., Balamurugan, V.: Finite element modelling of piezolaminated smart structures for active vibration control with distributed sensors and actuators. J. Sound Vibr. **262**, 529–562 (2003).
[10] Pinto Correia, I. F., Cristovao Mota Soares, M., Mota Soares Carlos, A., Herskovits, J.: Active control of axisymmetric shells with piezoelectric layers: a mixed laminated theory with a high order displacement field. Comput. Struct. **80**, 2265–2275 (2002).
[11] Wang, X. D., Huang, G. L.: Modelling and analysis of piezoelectric actuators in anisotropic structures. Acta Mech. **155**, 45–63 (2002).
[12] Sun, D., Tong, L.: Modal control of smart shells by optimized discretely distributed piezoelectric transducers. Int. J. Solids Struct. **38**, 3281–3299 (2001).
[13] Wang, C. Y., Vaicaitis, R.: Active control of vibrations and noise double wall cylindrical shells. J. Sound Vibr. **216**, 865–888 (1998).
[14] Zhang, X. N., Xie, S. L., Li, J. B., Zhang, J. H.: Experimental study of the controllable constrained damping layer structure with book-block actuator. J. Xi'an Jiaotong University **33**, 77–81 (1999) (In Chinese).
[15] Zhang, X. N., Li, Z. M., Zhang, J. H.: Book-block actuator and hybrid control of plate. Proceedings of ICAPV 2000, pp. 79–85. Beijing: Science Press 2000.
[16] Xie, S. L., Zhang, X. N.: Study on characteristic of book-block piezoelectric actuator. J. Vibr. Engng. **17**, 112–115 (2004) (In Chinese).